



ChemComm

Ethylene Oxide Functionalization Enhances Ionic Conductivity of a MOF

Journal:	<i>ChemComm</i>
Manuscript ID	CC-COM-03-2022-001286.R1
Article Type:	Communication

SCHOLARONE™
Manuscripts

COMMUNICATION

Ethylene Oxide Functionalization Enhances Ionic Conductivity of a MOF

Sorout Shalini^a and Adam J. Matzger^{*a,b}Received 00th January 20xx,
Accepted 00th January 20xx

DOI: 10.1039/x0xx00000x

Varying degrees of ethylene oxide (EO) functionalization of the zirconium MOF UiO-68 affords two novel MOFs; UiO-68-EO and UiO-68-2EO, exhibit solvent-free ionic conductivity upon loading LiTFSI in their pores. Incorporating EO chains provides a pathway for lithium ion migration between the coordinated sites and results in an ionic conductivity of 3.8×10^{-7} S/cm and 3.9×10^{-4} S/cm at 90 °C for UiO-68-EO/LiTFSI and UiO-68-2EO/LiTFSI respectively.

Solid-state batteries, batteries employing solid electrolyte systems, can achieve improved safety, stability, energy density, capacity, and are an enabling technology for lithium metal anodes.^{1,2} A variety of inorganic, organic, and inorganic–organic hybrid solid electrolytes have been developed and investigated.³ Although great advances have been made in the field, one of the fundamental challenges that remains is achieving acceptable ionic conductivity (10^{-2} to 10^{-3} S/cm) in these systems.^{4,5} Towards this goal, one promising approach shown to enhance ionic conductivity is to design salt-insulator composites with structural disorder at the salt-insulator interface.^{6,7} Metal-organic frameworks (MOFs) are ideal for such applications because confinement of salt in their ordered channels, which can potentially act as predesigned conduits for ion motion, inherently induces disorder at salt-insulator interfaces.^{8,9} We recently demonstrated this principle in observing a significant enhancement in ionic conductivity of tetraethylammonium bis(trifluoromethylsulfonyl)-imide ([NET₄][TFSI]) by confining it within an isorecticular series of zirconium-based MOFs: UiO-66, UiO-67, and UiO-68-(CH₃)₂ (i.e. PCN-56).¹⁰ The study found that the enhancement was dependent on the pore sizes within these 3-dimensional networks with the largest pore MOF, PCN-56, exhibiting the

maximum enhancement (factor of 50 relative to [NET₄][TFSI]). Extension of this approach to lithium bis(trifluoromethanesulfonyl)imide (LiTFSI) in PCN-56 (Fig. 1) was not successful due to low/negligible ion dissociation and resultant poor lithium ion transport. Ion dissociation and transport in LiTFSI-polymer composite systems has been widely investigated and research suggests that greater ion dissociation and mobility is facilitated via incorporation of chelating organic functionalities due to their propensity to interact with lithium ions.¹¹

Within LiTFSI-polymer composite systems, poly(ethylene oxide) (PEO) is the most widely researched solid electrolyte.¹² The well-established oxophilicity of lithium ions allows PEO, having a large number of donor oxygen atoms, to complex with LiTFSI and provide lithium ions with well-connected solvation shells, thus resulting in reasonable ionic conductivity.¹³ Additionally, the large TFSI anion size and its diffuse distribution of charge results in a uniform dispersion of LiTFSI within the PEO matrix.^{12,14} As lithium ion conductivity in these systems arises due to lithium-ethylene oxide (EO) interactions we hypothesized that incorporation of EO functionality within other systems, such as PCN-56/LiTFSI or UiO-68/LiTFSI (UiO-68 is isostructural to PCN-56; only difference being the absence of CH₃ groups on the linker),^{15,16} may have a similar effect. While introducing PEO into the pores of UiO-68 seems a straightforward approach, the reduction in pore volume, being occupied by polymer, would block the access of pores by LiTFSI and phase separation as a function of salt loading is a potential concern. Thus, a synthetic modification approach whereby EO chains were grafted onto the pore walls of UiO-68 was envisaged as providing the necessary lithium ion-EO interactions for increased ion dissociation and mobility while preserving pore space for improved ion migration—a truly hybridized approach. The ionic conductivity of the resulting functionalized MOFs was then compared to the conductivity of the PCN-56/LiTFSI. Though a prior covalent integration of EO chains within an anisotropic COF was shown to improve ionic conductivity in a LiClO₄ system,¹⁷ what remains unknown, and

^a Department of Chemistry, University of Michigan, 930 North University Avenue, Ann Arbor, MI 48109, USA.

^b Department of Macromolecular Science and Engineering, University of Michigan, Ann Arbor, MI 48019, USA.

†Electronic Supplementary Information (ESI) available: Experimental methods, synthesis of linkers and MOFs, NMR data, MOF and composite characterization, cyclic DSC of UiO-68-2EO/LiTFSI composites and Nyquist plot of UiO-68-2EO/LiTFSI/PC. See DOI: 10.1039/x0xx00000x

what is explored here: the degree of EO functionalization necessary to achieve improved MOF-composite solid electrolytes and the potential for a cubic host to provide omnidirectional ion transport.

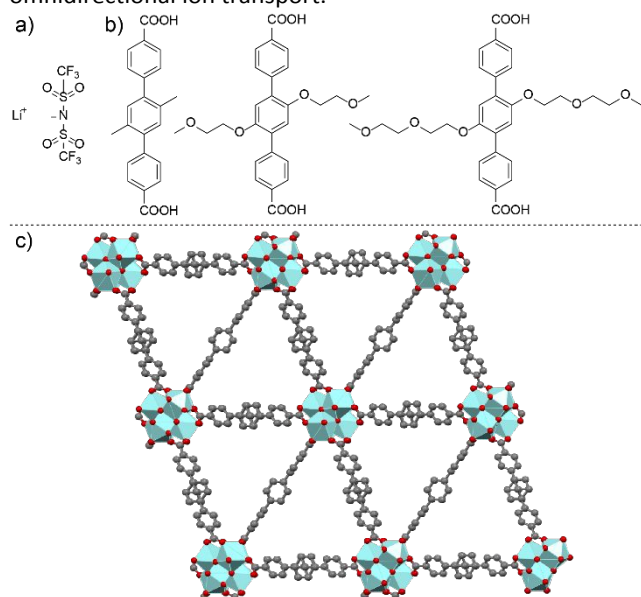


Figure 1. Structure of the a) salt LiTFSI b) linkers for PCN-56 (left), UiO-68-EO (middle), and UiO-68-2EO (right), and c) UiO-68.

Herein, we report two novel zirconium MOFs, UiO-68-EO and UiO-68-2EO, which are isostructural to PCN-56/UiO-68 and bear differing degrees of EO functionalization. These MOFs show enhanced ionic conductivity upon loading LiTFSI in their pores compared to the resistive PCN-56/LiTFSI composite. Incorporation of EO chains offers an improved pathway for transport of lithium ions, possibly by forming polyelectrolyte (Li-EO) interfaces within the MOF channels that assist ion dissociation of LiTFSI. The comparison of the conductivity for the two composites provides insight as to the optimum extent of EO functionality in such systems required to achieve good ionic conductivity.

Two novel linkers (Fig. 1b) were synthesized via Suzuki coupling of 1,4-dibromobenzene decorated with different length EO chains and 4-(methoxycarbonyl)phenyl)boronic acid (see ESI for detailed synthesis, and Fig. S2-S5 for NMR). These linkers were employed for the synthesis of two novel zirconium MOFs, UiO-68-EO and UiO-68-2EO, via solvothermal reaction with zirconium chloride, benzoic acid (modulator), and the linkers in DMF at 70 °C for 3-5 days. The MOFs are isostructural to PCN-56 and have $Zr_6O_4(OH)_4(O_2CR)_{12}$ nodes as well as a distribution of tetrahedral and octahedral pores. Powder X-ray diffraction (PXRD) patterns of UiO-68-EO and UiO-68-2EO match the PCN-56 pattern, and the BET surface areas determined by N_2 adsorption isotherms are 2535, and 1632 m^2g^{-1} , respectively (see ESI, Fig. S6 and S7). The increasing EO chain length from UiO-68-EO to UiO-68-2EO predictably leads to decreasing surface area and fractional void volume within the MOFs.

As prior work has shown that maximum conductivity in salt-loaded MOFs is achievable at just below the maximum possible salt loading,¹⁰ the theoretical maximum amount of LiTFSI that can be loaded in these MOFs was calculated using their

fractional void space accessible for loading and the density of pure LiTFSI (see ESI). The fractional void volume of UiO-68-EO and UiO-68-2EO was calculated theoretically; the change in volume associated with the linker changes (terphenyl dicarboxylate \rightarrow EO functionalized linkers, Fig. 1b) was calculated using the Spartan 18 software suite and subtracted from the fractional void volume of UiO-68, obtained via single crystal structure (refcode: UVUFEX) using Mercury, to arrive at the fractional void volume of UiO-68-EO (1.48 cc/g) and UiO-68-2EO (0.964 cc/g). The calculated void volumes are lower than the experimental pore volumes (UiO-68-EO-1.03 cc/g and UiO-68-2EO-0.841 cc/g) extracted from N_2 sorption isotherms at 77 K. Utilizing the calculated fractional void volume for each MOF, the maximum loadable amount of LiTFSI in UiO-68-EO and UiO-68-2EO was calculated to be 57.9% and 52.8% LiTFSI by mass. The vast majority of MOF-salt systems investigated for solid-state ion conduction report ionic conductivities that are assisted by solvent inclusion (see ESI). Solvent inclusion limits the battery operation to low temperatures; an inherent limitation of conventional liquid electrolytes.¹⁸ These solvents also tend to trigger undesirable interfacial side reactions with electrodes; therefore, we probe the enhancement in ionic conductivity without any contribution from organic solvents.¹⁹ To that end, LiTFSI was directly loaded into MOF pores post-synthetically via melting,²⁰ thus avoiding the incorporation of solvent. To ensure homogenous distribution the salt and activated MOF were ground together before heating the mixture at 235 °C, the melting point of LiTFSI. The salt in its molten state is absorbed into the MOF pores by capillary action.

The maximum experimental loading of LiTFSI in UiO-68-EO and UiO-68-2EO was determined by differential scanning calorimetry (DSC). The DSC trace of anhydrous LiTFSI (Fig. 2a) displays an endotherm at 163 °C corresponding to an irreversible solid-solid phase transition and a melt transition at 235 °C.²¹ Fig. 2b shows cyclic DSC for a physical mixture of 57.9% LiTFSI and 42.1% UiO-68-EO (calculated maximum loading of LiTFSI in UiO-68-EO) that is heated through three cycles from 30 °C to 250 °C at 10 °C min^{-1} with 5 min, 60 min, and 60 min hold at 250 °C, respectively. The endothermic phase transition and the melt endotherm observed at 155 °C and 209 °C during the first cycle disappear after the third cycle, which suggests that LiTFSI completely loads in the pores of MOF within \sim 2 hours. The absence of thermal events in the DSC trace after complete loading of salt in MOF is in accordance with the salt being unable to preserve its crystalline structure once inside the MOF pores (vide infra).^{10,20,22} However, a persistent melt endotherm and freeze exotherm is noted after heating the physical mixture of 60% LiTFSI and 40% UiO-68-EO (salt mass fraction slightly higher than the calculated maximum loading) for 24 hours indicating that there remains some LiTFSI external to the MOF pores unable to load (Fig. 2c). The maximum loading determined experimentally should be lower than the theoretical maximum because the salt should not be able to pack as densely in the MOF pores as it would in a pure crystal. However, for UiO-68-EO and UiO-68-2EO, the actual maximum loadings are in good agreement with the calculated values – a surprising result. More efficient packing of salt in these MOFs is

potentially aided by the polar environment and a high lithium ion solvation ability of EO units in the MOF.²³ Alternatively, the higher pore volume of the MOFs relative to the calculated fractional void volume suggests the presence of defects, missing-nodes and/or missing-linkers, within these MOFs (a common occurrence in UiO MOFs)^{24,25} explaining the slightly higher salt loading than the calculated value. Similar DSC experiments for physical mixtures of LiTFSI and UiO-68-2EO are presented in ESI (Fig. S8) validating the agreement between the calculated and experimental LiTFSI loading in UiO-68-2EO.

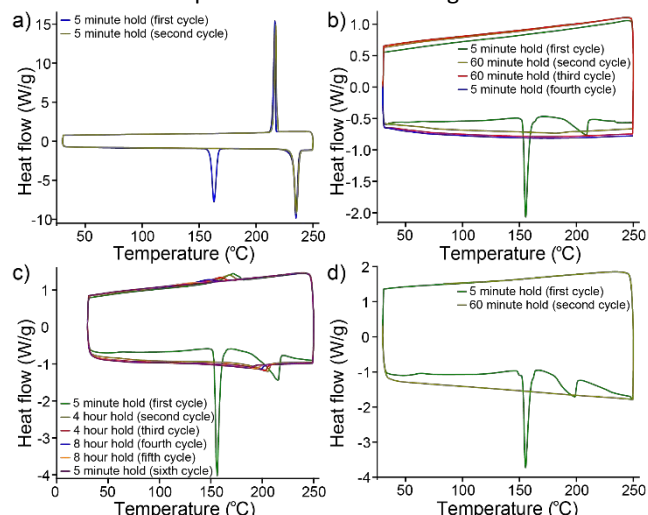


Figure 2. DSC traces of a) pure LiTFSI b) 57.9% LiTFSI in UiO-68-EO by mass, c) 60% LiTFSI in UiO-68-EO by mass, and d) 55.5% LiTFSI in UiO-68-EO by mass.

An established approach to improve ionic conductivity is to increase the charge carrier density by increasing the concentration of salt. It has been shown through experiment and molecular dynamics simulations that the ionic conductivity increases with increasing salt concentration and then starts to decrease after reaching a maximum due to an exponential increase in friction between the host and ions.^{10,14,26,27} The composites employed here to study the electrical properties of LiTFSI loaded in MOF are 55.5% LiTFSI, 44.5% UiO-68-EO and 50% LiTFSI, 50% UiO-68-2EO by mass (referred to as UiO-68-EO/LiTFSI and UiO-68-2EO/LiTFSI respectively from hereon). These mass fractions correspond to the amount of salt that is slightly less than what is required to completely fill the pores of each MOF. DSC experiments carried out on both composites confirm the absence of LiTFSI exterior to the MOFs (Fig. 2d and S7). PXRD patterns of these composites display diffraction peaks for MOFs but not for LiTFSI which indicates both complete LiTFSI loading into the MOFs and the absence of crystalline LiTFSI within the pores as well as the stability of these MOFs post salt loading (Fig. S9 and Fig. S10).

Electrochemical impedance spectroscopy (EIS) was performed for the composites as well as pure LiTFSI at temperatures varying from 40 °C to 90 °C (see ESI for more details). The Nyquist plots for the two composites recorded as a function of temperature, shown in Fig. 3a and 3b, exhibit a semicircle in the high frequency region followed by a capacitive tail in low frequency region. The calculated conductivities increase with temperature (Fig. 3c, Table S1 and S2). Pure LiTFSI was found to

be resistive, and the impedance values obtained at different temperatures matched the capacitance of our test cell.

UiO-68-EO/LiTFSI and UiO-68-2EO/LiTFSI exhibit an ionic conductivity of 3.8×10^{-7} S/cm and 3.9×10^{-4} S/cm at 90 °C, respectively. Both composites show enhanced conductivity when compared to pure LiTFSI as well as PCN-56/LiTFSI. The incorporation of EO chains provides a pathway for lithium ion conduction through these MOFs as the lithium ions migrate between the coordinated sites. UiO-68-2EO/LiTFSI, having greater EO functionalization, shows higher conductivity than UiO-68-EO/LiTFSI. The main difference between UiO-68-EO and UiO-68-2EO is the length of the EO chains lining the MOF pores and this is likely the cause of the difference in ionic conductivity. The higher EO/pore functionalization ratio in UiO-68-2EO provides improved solvation of LiTFSI and affords an improved pathway for lithium ion migration via favorable electrostatic lithium ion–oxygen interactions. However, a recent study touched on the relationship between the stoichiometric ratio of oxygen/carbon ($p = [O]/[C]$) and ionic conductivity within a polymer-LiTFSI composite system and established an inverse correlation between ionic conductivity and p .²⁸

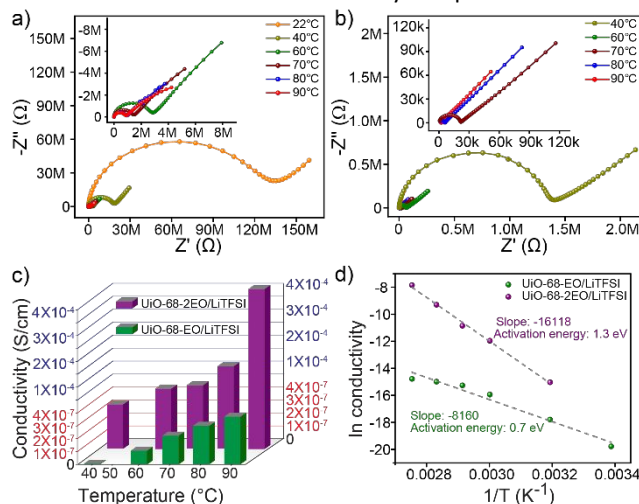


Figure 3. Nyquist plots for a) UiO-68-EO/LiTFSI at temperatures from 22 °C to 90 °C, and b) UiO-68-2EO/LiTFSI at temperatures from 40 °C to 90 °C. c) Plot comparing the conductivity of UiO-68-EO/LiTFSI and UiO-68-2EO/LiTFSI at different temperatures. *Note the different scales for conductivity shown in red and blue. (d) Arrhenius plots for the conductivity of UiO-68-EO/LiTFSI and UiO-68-2EO/LiTFSI.

The data presented in the study suggests that there is a maximum achievable improvement via EO-assisted ion solvation, and functionalization beyond this threshold (defined here as “critical p ”) impedes ion mobility. Increasing the chain length (EO functionalization) from UiO-68-EO to UiO-68-2EO decreases the value of p (UiO-68-EO $p = 0.67$, UiO-68-2EO $p = 0.60$) leading to a greater enhancement in ionic conductivity for UiO-68-2EO/LiTFSI and demonstrates that this degree of functionalization remains above critical p . Additionally, the conductivity of UiO-68-2EO/LiTFSI is found to be comparable to the conductivity of PEO/LiTFSI composites which vary from 10^{-3} S/cm to 10^{-5} S/cm depending on the plasticizer used and the temperature of measurement.¹² Ionic conductivity similar to PEO/LiTFSI and other MOF/Li salt systems (Table S3) is achieved in UiO-68-2EO/LiTFSI without a plasticizer or any additive

contributing to conductivity, a demonstrable improvement upon contemporary composite technologies.

Among other factors contributing to the efficacy of solid electrolyte battery systems, the activation energy for ion migration is an important consideration with implications for total accessible energy within a system. Fig. 3d presents Arrhenius plots for the conductivity of UiO-68-EO/LiTFSI and UiO-68-2EO/LiTFSI. The calculated activation energy of conductivity from the Arrhenius plot for UiO-68-EO/LiTFSI is 0.76 eV, compared to 1.3 eV for UiO-68-2EO/LiTFSI. For UiO-68-EO/LiTFSI to have a significantly lower activation energy than that of UiO-68-2EO/LiTFSI, despite having a conductivity that is 3 orders of magnitude lower, indicates weaker interactions of UiO-68-EO with salt. This is consistent with the presence of fewer oxygen atoms (lower EO functionalization) in UiO-68-EO as the mobility of lithium ions would be affected by the interaction between lithium ions and EO units (more interactions would add to activation energy) in addition to the degree of the dissociation of LiTFSI. The calculated activation energies for these composites are higher than previously reported MOF-based solid-state Li-ion conductors (Table S3). This may be attributed to the inclusion of solvent within those systems, possibly signifying a solvent dominant conduction pathway. By increasing *p*, conductivity is sacrificed but activation energy is depressed. We propose that optimizing the degree of EO functionalization cannot be independently considered and developing an EO-functionalized MOF system for use as a solid electrolyte will require consideration of both the degree of EO functionalization and *p*. Balancing these apparently at-odds metrics will allow the design of composites with desirably high conductivity and low activation energy.

Conclusions

The presence of polar oxygen functionalities within UiO-68-EO and UiO-68-2EO due to grafted EO chains provides a tight, well-knit three-dimensional pathway for the transport of lithium ions. The measure of conductivity for these composites is influenced by the number of EO units present in the system. More EO units provide well-connected solvation sites for conduction of lithium ions via chain-hopping which leads to a higher conductivity. However, the increase in ionic conductivity comes with a trade-off in activation energy since presence of more EO units essentially requires greater energy for Li-O dissociation which increases the activation energy. Towards addressing this, at this time it is understood that there is a lower energy barrier for intra-EO chain lithium ion transfer than the inter-chain counterpart.²⁹ Therefore, an optimal EO-MOF functionalization strategy may involve increased EO chain length coupled with a decrease in the number of chains occupying each MOF pore. Such an arrangement may achieve optimal *p* while also minimizing the energy required for the processes of lithium ion migration.

The manuscript was written through contributions of all authors. All authors have given approval to the final version of the manuscript. The authors would like to thank Chris Swendris for his assistance with linker synthesis.

This work was supported as part of the Joint Center for Energy Storage Research (JCESR), an Energy Innovation Hub funded by the U.S. Department of Energy, Office of Science, Basic Energy Sciences. There are no conflicts to declare.

Notes and references

- 1 Y. Horowitz, C. Schmidt, D. Yoon, L. M. Riegger, L. Katzenmeier, G. M. Bosch, M. Noked, Y. Ein-Eli, J. Janek, W. G. Zeier, C. E. Diesendruck, D. Golodnitsky, *Energy Technol.* 2020, **8** (11), 2000580.
- 2 D. Lin, Y. Liu, Y. Cui, *Nat. Nanotechnol.* 2017, **12** (3), 194.
- 3 W. Zhao, J. Yi, P. He, H. Zhou, *Electrochem. Energy Rev.* 2019, **2** (4), 574.
- 4 A. Manthiram, X. Yu, S. Wang, *Nat. Rev. Mater.* 2017, **2** (4), 1.
- 5 L. Wang, J. Li, G. Lu, W. Li, Q. Tao, C. Shi, H. Jin, G. Chen, S. Wang, *Front. Mater.* 2020, **7**, 111.
- 6 C. C. Liang, *J. Electrochem. Soc.* 1973, **120** (10), 1289.
- 7 J. Maier, *Prog. Solid State Chem.* 1995, **23** (3), 171.
- 8 Z. Wang, R. Tan, H. Wang, L. Yang, J. Hu, H. Chen, F. Pan, *Adv. Mater.* 2018, **30** (2), 1704436.
- 9 Z. Wang, Z. Wang, L. Yang, H. Wang, Y. Song, L. Han, K. Yang, J. Hu, H. Chen, F. Pan, *Nano Energy* 2018, **49**, 580.
- 10 S. Shalini, T. P. Vaid, A. J. Matzger, *Chem. Commun.* 2020, **56** (53), 7245.
- 11 N. S. Schausser, A. Nikolaev, P. M. Richardson, S. Xie, K. Johnson, E. M. Susca, H. Wang, R. Seshadri, R. J. Clément, J. Read de Alaniz, R. A. Segalman, *ACS Macro Lett.* 2021, **10** (1), 104.
- 12 Z. Xue, D. He, X. Xie, *J. Mater. Chem. A* 2015, **3** (38), 19218.
- 13 C. Fang, W. S. Loo, R. Wang, *Macromolecules* 2021, **54** (6), 2873.
- 14 O. Borodin, G. D. Smith, *Macromolecules* 2006, **39** (4), 1620.
- 15 J. H. Cavka, S. Jakobsen, U. Olsbye, N. Guillou, C. Lamberti, S. Bordiga, K. P. Lillerud, *J. Am. Chem. Soc.* 2008, **130** (42), 13850.
- 16 H.-L. Jiang, D. Feng, T.-F. Liu, J.-R. Li, H.-C. Zhou, *J. Am. Chem. Soc.* 2012, **134** (36), 14690.
- 17 Q. Xu, S. Tao, Q. Jiang, D. Jiang, *J. Am. Chem. Soc.* 2018, **140** (24), 7429.
- 18 M. Alipour, C. Ziebert, F. V. Conte, R. Kizilel, *Batteries* 2020, **6** (3), 35.
- 19 K. Xu, *Chem. Rev.* 2014, **114** (23), 11503.
- 20 S. Seth, T. P. Vaid, A. J. Matzger, *Dalton Trans.* 2019, **48** (35), 13483.
- 21 W. A. Henderson, D. M. Seo, Q. Zhou, P. D. Boyle, J.-H. Shin, H. C. De Long, P. C. Trulove, S. Passerini, *Adv. Energy Mater.* 2012, **2** (11), 1343.
- 22 K. Fujie, T. Yamada, R. Ikeda, H. Kitagawa, *Angew. Chem.* 2014, **126** (42), 11484.
- 23 G. Zhang, Y. Hong, Y. Nishiyama, S. Bai, S. Kitagawa, S. Horike, *J. Am. Chem. Soc.*, 2019, **141**(3), 1227.
- 24 G. C. Shearer, S. Chavan, J. Ethiraj, J. G. Vitillo, S. Svelle, U. Olsbye, C. Lamberti, S. Bordiga, K. P. Lillerud, *Chem. Mater.* 2014, **26** (14), 4068.
- 25 L. Liu, Z. Chen, J. Wang, D. Zhang, Y. Zhu, S. Ling, K.-W. Huang, Y. Belmabkhout, K. Adil, Y. Zhang, B. Slater, M. Eddaoudi, Y. Han, *Nat. Chem.* 2019, **11** (7), 622.
- 26 G. Mao, M. L. Saboungi, D. L. Price, M. Armand, F. Mezei, S. Pouget, *Macromolecules* 2002, **35** (2), 415.
- 27 S. Lascaud, M. Perrier, A. Vallee, S. Besner, J. Prud'homme, M. Armand, *Macromolecules* 1994, **27** (25), 7469.
- 28 R. L. Snyder, Y. Choo, K. W. Gao, D. M. Halat, B. A. Abel, S. Sundararaman, D. Prendergast, J. A. Reimer, N. P. Balsara, G. W. Coates, *ACS Energy Lett.* 2021, **6** (5), 1886.
- 29 D. J. Brooks, B. V. Merinov, W. A. Goddard, B. Kozinsky, J. Mailoa, *Macromolecules* 2018, **51** (21), 8987.